# Analysis of a micro vertical-axis wind turbine by computational fluids simulation

Ramón Jaramillo-Martínez, Manuel Reta-Hernández (*SM, IEEE*), Hector R. Vega-Carrillo (*M, IEEE*),
Jorge de la Torre y Ramos and Francisco Bañuelos-Ruedas
Universidad Autónoma de Zacatecas
Unidad Académica de Ingeniería Eléctrica
Av. López Velarde No. 801, Zacatecas, Zac, 98000, México
jaramillo.ramon@hotmail.com mretah@uaz.edu.mx fermineutron@yahoo.com jorgetorre@uaz.edu.mx fbanuelosrs@hotmail.com

***Abstract*—The installed capacity of wind energy around the world using big horizontal-axis wind turbines (HAWT) has grown substantially in the last two decades. Likewise, research and development of vertical-axis wind turbines (VAWT) for small power applications has been increased during the last seven years. This paper presents the performance analysis related to the power output of a micro VAWT with three blades in helicoidal form, based on computacional fluids dynamics simulation (CFD), using *Ansys Fluent*®. In the analysis, several parameters related to the aerodynamic performance were varied, keeping constant the sweeping area. To compare results, a mathematical model was created in *Matlab*®, using the double-multiple streamtube method (DMST), which considers variations in relative wind speed through the wind turbine. Results from both, CFD simulation and DMST model, applied to the micro turbine are presented.**

***Index terms*—Vertical-axis wind turbine; Helical form; Darrieus; Double-multiple streamtube.**

## I. Introducción

The anthropogenic contribution to the global warming, due to the use and energy production, is nowadays one of the most important environmental issues [1]. The greenhouse gas emission, like $CO_2$, $NO_x$ and methane have been related to the global warming. The anthropogenic CO2 emissions are mainly due to the fossil fuel use for power production [2].

The renewable sources are a technological solution to reduce the use of fossil fuels for power production. Wind energy has been one of the most developed renewable source around the world, reaching competitive costs per $kWh$ generated in big HAWTs, compared to those in fossil fuel-based plants. By June 2014, the world installed wind power capacity was of 336,327 $MW$, where China, USA, Germany, Spain, and India account for 72% of the total [3].

Small wind turbines (SWT) may have either vertical or horizontal axis. Although there is not a unique definition for SWT, the International Electrotechnical Commission (IEC) defines it as a turbine having a rotor swept area of less than 200 $m^2$, equating to a rated power of approximately 50 $kW$, generating at a voltage below 1,000 $Vac$ or 1,500 $Vdc$. However, several countries have their own definition of SWT. The discrepancy of the upper capacity limit of SWT ranges between 15 $kW$ to 100 $kW$ for the five largest small wind countries. The HAWT technology has dominated the market for over 30 years. Based on the study of 327 SWT manufacturers at the end of 2011, 74% invested in the horizontal axis orientation, 18% adopted the vertical design, and 6% worked with both technologies [4].

Most of the small vertical-axis wind turbines (SVAWTs) have been developed in the last seven years, mainly for stand-alone applications, and their market share still remains relatively small. The average rated capacity of SVAWTs is estimated to be 7.4 $kW$ with a median rated capacity of 2.5 $kW$. In comparison with the traditional horizontal axis orientation, the average and median rated capacity are much smaller [4]. The rated capacity of SVAWTs below 1 $kW$ may be considered as micro vertical-axis wind turbines (micro VAWT). The inclusion of computational fluid dynamics (CFD) into wind energy technology has facilitated the design of new prototypes of wind turbines.

In this paper, it is presented the analysis of a micro VAWT with helical form in their blades, based on a mathematical model, and validated with CFD.

## II. Background

### A. Darrieus-type VAWT

The Darrieus-type VAWT was patented by George Jeans Mary Darrieus in 1925 in France, and in 1931 in the United States. Both patents covered two main configurations, curved and straight blades, as shown in Fig. 1. The Darrieus-type VAWT is a lift force driven wind turbine with two or more aerofoil-shaped blades attached to a rotating vertical shaft. The wind blowing over the aerofoil contours of the blade creates aerodynamic lift that actually pulls the blades along [5].

To improve the performance of the Darrieus-type turbine, various modifications have been proposed over the time. Fig. 2 shows the development of the Darrieus wind turbine, according to Tjiu [6]. The main variations on turbine with curved blades, known as *phi-rotor* or *egg-beater*, are the *guy-wired*,

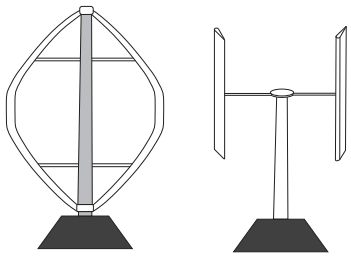

Fig. 1. Curved and straight-blades configurations of Darrieus VAWT [6].

978-1-4673-7121-6/15/$31.00 

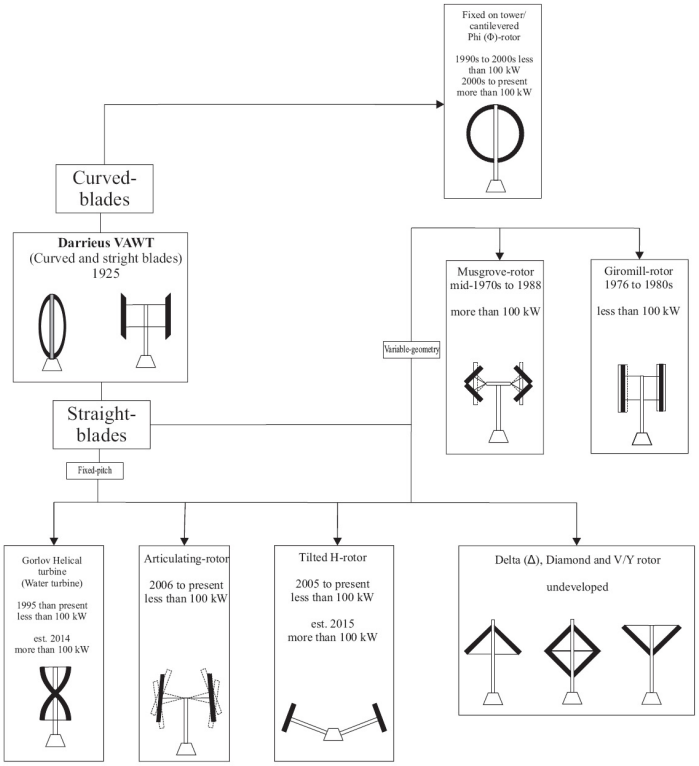


Fig. 2. Time line of the Darrieus-type vertical-axis wind turbine [6].

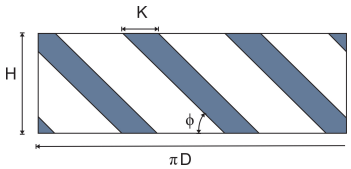


Fig. 3. Projection of helical turbine blades on a vertical plane [6].

the *fixed-on tower*, and the *cantilevered* versions. Similarly, the variations on straight blades configurations are known as *diamond*, *V/Y*, *delta (Δ)* and *Musgrove-rotor*.

### B. Gorlov or helical turbine

The Gorlov or helical turbine was proposed in 1995 by A.M. Gorlov, at the Northeastern University, in Boston, USA, introducing twisting to the blades of the straight-blade VAWT along the perimeter to get helicoidal shape.The main purpose was to improve torque distribution and to reduce fatigue and noise. Fig. 3 shows a projection of the blades on a vertical plane. The inclination angle of the blades is expressed in (1), where $N$ is the amount of blades, $H$ is the rotor height, and $D$ is the turbine diameter [7]-[9].

$$\phi = \tan^{-1}\left(\frac{NH}{\pi D}\right) \tag{1}$$

### C. Extracted power of wind turbines

The thrust force, $F_T$, the torque, $T_t$, and the power delivered, $P_t$, in a wind turbine, are expressed in terms of thrust, torque, and power coefficients respectively, $C_T$, $C_Q$, and $C_P$, as shown in (2)-(4) [10].

$$F_T = \frac{1}{2}\rho\, V_\infty^2\, A\, C_T(\lambda,\beta) \tag{2}$$

$$T_t = \frac{1}{2}\rho\, V_\infty^2\, A\, C_Q(\lambda,\beta) \tag{3}$$

$$P_t = \frac{1}{2}\rho\, V_\infty^3\, A\, C_P(\lambda,\beta) \tag{4}$$

where:
$V_\infty$ = apparent wind speed, in $m/s$.
$\rho$ = air density, in $kg/m^3$.
$A = HD$ = swept area, in $m^2$.
$\beta$ = inclination angle, in $degrees$.
$\lambda$ = tip speed ratio.

The average torque, $\overline{T_t}$, of a wind turbine is the arithmetic mean of one revolution, expressed in (5), where $\theta$ is the azimuth angle [10]. The power delivered by the turbine, $P_t$, is defined by (6), where $\omega$ is the rotational speed in $rad/s$.

$$\overline{T_t} = \frac{1}{2\pi}\int_0^{2\pi} T_t(\theta)\; d\theta \tag{5}$$

$$P_t = \omega\; \overline{T_t}\; N \tag{6}$$

Tip-speed-ratio (TSR) or $\lambda$, is an important parameter defined as the ratio of the speed of the blade tip and the wind speed, both in $m/s$, expressed in (7), where $R$ is the radius of the turbine, in $m$. Solidity, $\sigma$, is defined as the ratio between the length of the blade chord and the radius of the turbine, expressed in (8), where $K$ is the blade chord, in $m$ [11].

$$\lambda = \frac{\omega\; R}{V_\infty} \tag{7}$$

$$\sigma = \frac{N\; K}{R} \tag{8}$$

### D. Mathematical model of the proposed micro turbine

There are several mathematical models proposed in literature to calculate the aerodynamic performance of VAWTs, highlighting the single streamtube model (SST), the multiple streamtube model (MST) and the double-multiple streamtube model (DMST) [12]-[14]. This paper used the DMST model to analyze the micro turbine performance.

### E. Double-multiple streamtube model

The double-multiple streamtube model was introduced in 1981 by Paraschivoiu [15] to predict the performance of a Darrieus wind turbine. In the model, the turbine is represented by a pair of actuator disks in tandem at each level of the rotor. The concept of the two actuator discs in tandem for a Darrieus wind turbine was originally given by Lapin [16].

The different induced velocities are considered at the upstream and downstream haves of the rotor swept volume. The flow through the turbine is divided into a large number of streamtubes, each one having aerodynamic independence. The freestream speed is obtained with (9) [12]-[17].

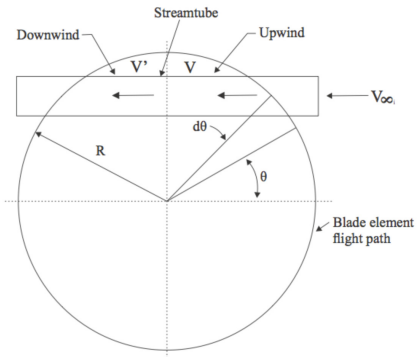


(a) Plant View.

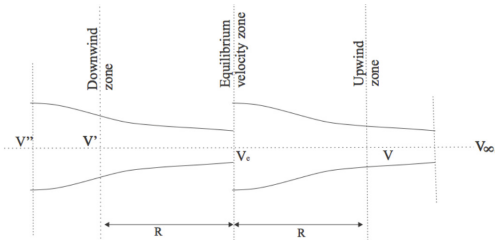


(b) Rotor element replaced by two actuador disks in tandem.

Fig. 4. Schematics of the DMST model (CARDAA code) [17].

$$\frac{V_{\infty i}}{V_\infty} = \left(\frac{Z_i}{Z_{EQ}}\right)^{\alpha_W} \tag{9}$$

where:
$V_{\infty i}$ = local freestream wind speed, vertical direction, in $m/s$,
$V_\infty$ = freestream wind speed, in $m/s$.
$Z_i$ = local turbine height, in $m$.
$Z_{EQ}$ = local turbine height at the equator, in $m$.
$\alpha_W$ = atmospheric wind shear exponent.

The flow in each streamtube interacts in both actuators disks; the first disk includes the upwind half of the surface swept by the rotor ($-\pi/2 \leqslant \theta \leqslant \pi/2$) and the second disc includes the downwind half ($\pi/2 \leqslant \theta \leqslant 3\pi/2$), as shown in Fig. 4. As a result, the induced velocity decreases on both discs, which better approximates the model.

Throughout the multiple columns, it can be assumed five different speeds. Taking $V_\infty$ as a reference, the local ambient wind speed, $V$, seen by the turbine is obtained by multiplying the freestream wind speed by an interference factor $u$. This is done in both actuators discs, as expressed in (10)-(13) [12]-[17].

$$V = uV_{\infty_i} \tag{10}$$
$$V_e = (2u-1)V_{\infty_i} \tag{11}$$
$$V' = u'V_e = u'(2u-1)V_{\infty_i} \tag{12}$$
$$V'' = (2u-1)(2u'-1)V_{\infty_i} \tag{13}$$

where:
$V_e$ = induced equilibrium velocity, in $m/s$.
$V', V''$ = upwind and downwind induced velocities, in $m/s$.
$u, u'$ = upwind and downwind interference factors.

The local relative wind speed, $W$, in the first half of the rotor, and the angle of attack, $\alpha$, are given by (14) and (15). Their corresponding values in the second half of the rotor, $W'$, and $\alpha'$, are represented as a function of $\lambda'$ as in (14) and (15) [10]-[11].

$$W^2 = V^2\left[(\lambda - \sin(\theta))^2 + \cos^2(\theta)\cos(\delta)\right] \tag{14}$$

$$\alpha = \sin^{-1}\left[\frac{\cos(\theta)\cos(\delta)}{\sqrt{(\lambda - \sin(\theta))^2 + \cos^2(\theta)\cos(\delta)}}\right] \tag{15}$$

The coefficients for normal and tangential forces, $C_N$ and $C_T$, are expressed in (16) and (17) [12]-[13]. The lift and drag coefficients, $C_L$ and $C_D$, are obtained from to the angle of attack and Reynolds number for a given airfoil.

$$C_N = C_L\cos(\alpha) + C_D\sin(\alpha) \tag{16}$$
$$C_T = C_L\sin(\alpha) - C_D\cos(\alpha) \tag{17}$$

The average torque coefficients in both zones are obtained with (18) and (19) [12]-[13]. The turbine power coefficient, $C_P$, is the sum of power in both discs, expressed in (20).

$$\overline{C_Q} = \frac{NKh}{2\pi A}\int_{-\frac{\pi}{2}}^{\frac{\pi}{2}}\int_{-1}^{1} C_T\left(\frac{W}{V_\infty}\right)^2\frac{\eta}{\cos\delta}\,d\zeta\,d\theta \tag{18}$$

$$\overline{C'_Q} = \frac{NKh}{2\pi A}\int_{\frac{\pi}{2}}^{\frac{3\pi}{2}}\int_{-1}^{1} C_T\left(\frac{W'}{V_\infty}\right)^2\frac{\eta}{\cos\delta}\,d\zeta\,d\theta \tag{19}$$

$$C_P = \left(\overline{C_Q} + \overline{C'_Q}\right)\lambda \tag{20}$$

where:
$\delta$ = angle between the blade normal and the equatorial plane, in $degrees$.
$\theta$ = azimuthal angle, in $degrees$.
$\eta = r/R$. $R$ is the rotor radius at the equator, and $r$ is the local rotor radius, both in $m$.
$\zeta = z/h$. $z$ is local turbine height, and $h$ is the half height of the rotor, both in $m$.

### *F. Computational fluids dynamic (CFD)*

Navier-Stokes equations, given in (21)-(23), express the principles of conservation of mass, movement quantity and energy of any fluid in partial differential equations form. These equations are used in commercial fluid dynamics software, replacing a problem defined in continuos domain by one in discrete domain from a given mesh [19]-[20].

$$\frac{\partial\rho}{\partial t} + \nabla\cdot(\rho\vec{v}) = 0 \tag{21}$$

$$\rho\frac{\partial\vec{v}}{\partial t} + \rho(\vec{v}\cdot\nabla)\vec{v} = -\nabla p + \rho\vec{g} + \nabla\cdot\tau_{ij} \tag{22}$$

$$\rho\frac{\partial E}{\partial t} + \rho\nabla\cdot(\vec{v}E) = \nabla\cdot(k\nabla T) + \rho\vec{g} + \\ +\nabla\cdot(\overrightarrow{\sigma}\cdot\vec{v}) + \dot{W}_f + \dot{q}_H \tag{23}$$

where:
$\rho$ = fluid density, in $kg/m^3$,

$\vec{v}$ = velocity vector, in $m/s$,
$t$ = time, in $s$,
$\vec{g}$ = gravitational vector, in $m/s^2$,
$\tau_{ij}$ = Reynolds stress,
$p$ = fluid pressure, in $Pa$,
$E$ = activation energy, in $kJ/mol$,
$k$ = thermal conductivity coefficient, in $W/(m\ ^oK)$,
$\overrightarrow{\sigma}$ = stress tensor,
$W_f$ = fluid power, in $watts$,
$q_H$ = heat exchanged by mass unit, in $joules$.

*1) Turbulence model:* In CFD simulation, the turbulence is considered with different approaches. The k-omega model ($k\omega$) is one of the most appropriate method in analysis of turbulent flow for low Reynolds numbers, and it presents different sub-models to include effects of compressibility and shear stresses correction. The shear stress transport model (SST) ($k\omega$) is widely used in simulation of wind turbines because it produces more accurate and reliable results [18]-[19].

## III. Study Case

The performance analysis was applied on a micro VAWT with blades in helical shape, assuming a rated output power of 450 $W$ at a wind speed of 7.5 $m/s$. The air density was considered at sea level ($\rho = 1.225\ kg/m^3$), assuming a $C_P = 0.3$. The estimated swept area of the turbine was 5.8 $m^2$.

### A. Applying the DMST model

Based on the literature, it was developed a *Matlab*® code to calculate the turbine power coefficient, and applied to the study case [13]. The results were later compared to the results obtained in an experimental model performed by Castelli [20], similar to the proposed one.

To select the appropriate design parameters for the turbine, a numerical optimization of each parameter was carried out at constant swept area, so the variation of the power coefficient for each case could be tested, as a function of the tip speed ratio.

### B. Applying computational fluids dynamic simulation

The computational fluid dynamic simulations were performed on the *Fluent ANSYS Inc.*® software package, for different solidity values (chord and number of blades) to determine its aerodynamic performance. The simulations were performed taking different values of tip speed ratio, to obtain the velocity and pressure fields and, therefore, the aerodynamic forces and moments. With all this, it was possible to generate $C_P$ curves as a function of $\lambda$.

As helical-type turbine is a variation of the H-type turbine, two-dimensional simulations were performed on the H-type turbine to find its optimal design parameters, and then applied torsion to the blades for achieving the helicoidal turbine model. Three-dimensional simulation was necessarily performed later on helical-type turbine due to the shape.

Mohamed [18] performed computer simulations on 20 symmetric and asymmetric aerodynamic profiles of a Darrieus-type, straight-blades, vertical turbine, showing that symmetrical profiles have better performance, unlike blades profiles

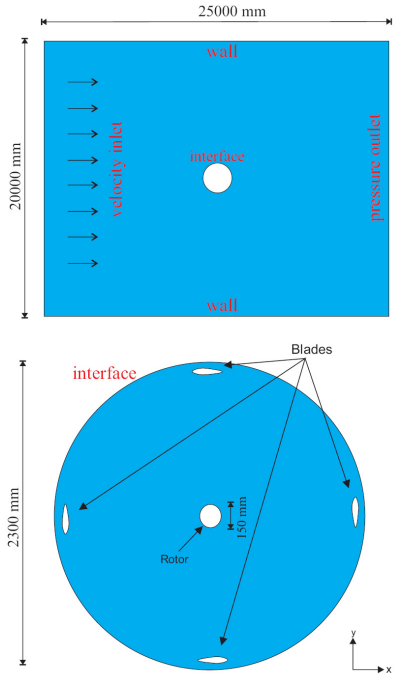


Fig. 5. Geometry used for the computational fluid dynamic simulation.

TABLE I. Mesh Characteristics

| Parameter | Value |
|---|---|
| Mesh quality | Fine |
| Curvature normal angle | 18° |
| Smoothing | High |
| Proximity accuracy | 0.5 |
| Number of cells across gap | 3 |
| Minimum size | $4.67 \times 10^{-3}\ m$ |
| Maximum size | 0.9347 $m$ |
| Growth rate | 1.2 |

of horizontal axis turbines. For the study case, it was chosen the symmetric S-1046 profile. All simulations were performed considering both, rotary and static domain, as shown in Fig. 5. The characteristics used in the mesh for simulation are shown in Table I.

The simulations performed to obtain the aerodynamic characteristics of different configurations were taken with time step size of 0.001 $s$ up to 3 revolutions. The number of time steps were equal to $6\pi/(0.001\ \omega)$. The coupling method between pressure and speed is called Semi-Implicit Method for Pressure-Linked Equations (SIMPLE). The spatial discretizations of pressure, moment, turbulence kinetic energy, $k$, specific dissipation rate turbulence, $\epsilon$, and energy, were all of first order.

The boundary conditions used for all simmulations are summarized in Table II.

TABLE II. Boundary Conditions.

| Indicator | Value |
|---|---|
| Wind speed | 7.5 $m/s$ |
| Air density | 1.225 $kg/m^3$ |
| Pressure | 101325 $Pa$ |
| Turbulence intensity | 5 % |
| Length scale of turbulence | 1 $m$ |

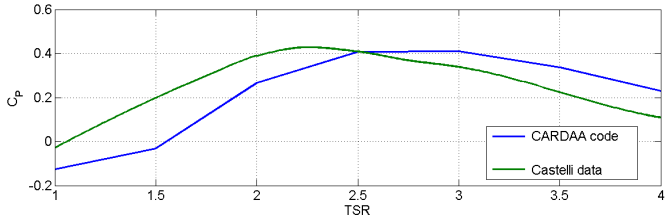


Fig. 6. Results from CARDAA code in *Matlab*® and Castelli [20].

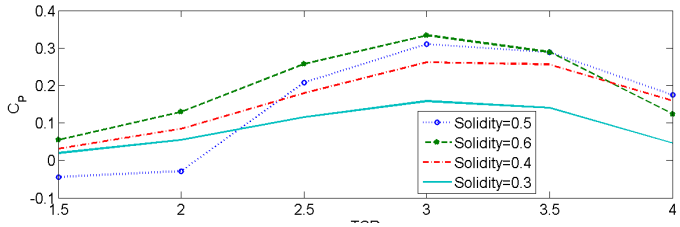


Fig. 7. $C_P$ versus $TSR$ ($\lambda$) with different solidity values in 3 blades.

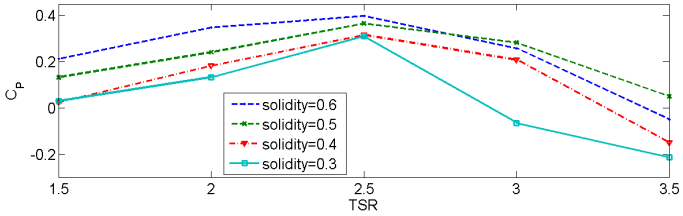


Fig. 8. $C_P$ versus $TSR$ ($\lambda$) with different solidity values in 4 blades.

## IV. Results

In Fig. 6 are shown $C_P$ values versus $\lambda$ or TSR, obtained from the mathematical model code, compared to the results obtained in similar experimental modeling reported by Castelli [20]. It can be observed similarity in the trend of the power coefficient path. Although there is an average statistical error of 16 %, the code algorithm allows a rapid estimation of turbine efficiency, which represents reduction of simulation time.

As mentioned earlier, solidity is a dimensionless parameter which directly influences the aerodynamic performance; that is why fluid dynamics simulations for different solidity values on 3 and 4 blades were performed. The simulation results are shown in Fig. 7 and 8, where it can be seen that, regardless of the number of blades, a higher solidity value determines a higher power coefficient, and increases the operating range of the turbine. The maximum power coefficient for both turbines is achieved with a solidity value of 0.6; however, the operating range starts decreasing from that value. For 3 blades, the maximum efficiency is 0.39 with $\lambda = 2.5$. The best performance for 4 blades is 0.36 for $\lambda = 3$. The operating range is wider for 3 blades.

Fig. 9 shows the angle of attack versus the azimuthal position of the blade for different values of $TSR$. For $\lambda = 1$, the angle of attack takes undesirable high values, causing poor stability to the blades, and delivering negative power coefficient values. As TSR increases, the range of values of the angle of attack decreases, for more stable conditions, and thus better performance.

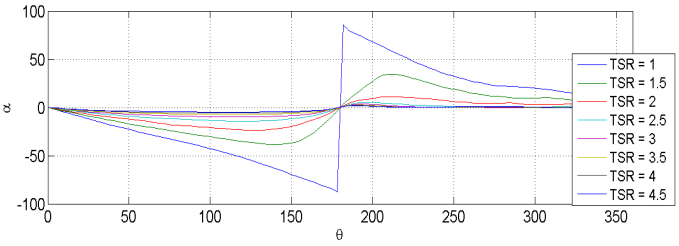


Fig. 9. Angle of attack ($\alpha$) versus azimuth angle ($\theta$) with different $\lambda$ values.

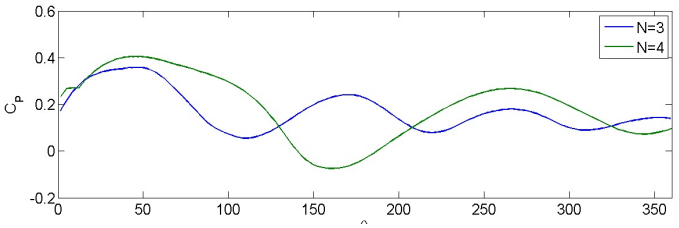


Fig. 10. Power coefficient ($C_P$) versus azimuth angle ($\theta$) for 3 and 4 blades.

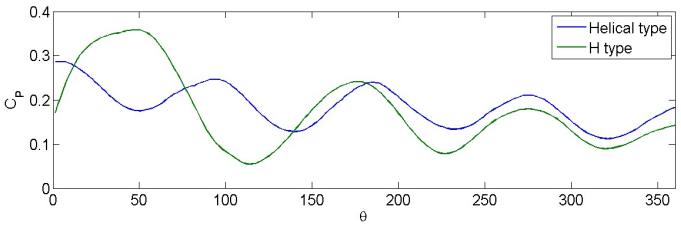


Fig. 11. $C_P$ versus $\theta$ for helical-type and H-type turbines.

Based on the above, it is easy to understand that the power coefficient is affected by the azimuth position of the blades. Fig. 10 shows the power coefficient versus the azimuth angle for 3 and 4 blades along one revolution.

As lift and drag coefficients depend on the angle of attack, the power coefficient varies depending on the azimuthal position. Turbines with 3 and 4 blades show a decline in the power coefficient starting from 60º; For 3-blades case, the minimum value of 0.07 is reached at an angle of 115º. For 4-blades case, its lowest point of -0.08 is reached at an angle of 160º. Despite the 4-blades turbine reaches a higher $C_P$ value, the average in one revolution is lower due to some negative values in the range of 145º to 185º. However, the 4-blades turbine presents a better starting in the range of 0º to 60º.

For a better torque distribution and to reduce fatigue, the helical-type turbine is preferred. Fig. 11 shows comparison on the performance of H-type and helical-type turbines. It can seen that in the helical turbine the power coefficient as a function of azimuthal angle has less variations along one revolution; moreover, the average power coefficient has an increment of 0.06% and it does not fall to critical areas or "dead zones", which performs better for areas where the variation in wind direction is constant.

Fig. 12 shows comparison between H-type and helical-type turbines, displaying results from the mathematical model and the simulations. The results trends from both types of analysis show similarity in both turbines. The results from

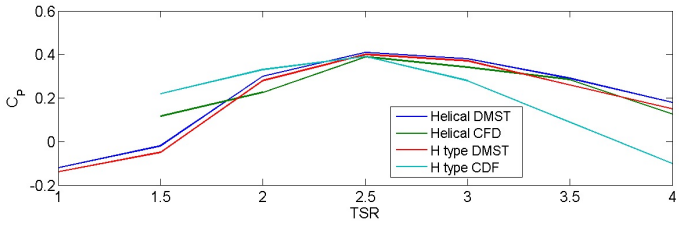


Fig. 12. $C_P$ versus $TSR$ for helical-type and H-type turbines, using mathematical model and CFD simulation.

TABLE III. PARAMETERS OF FINAL ROTOR DESIGN.

| Parameter | Value |
|---|---|
| Radio | 1 $m$ |
| Height | 2.9 $m$ |
| Solidity | 0.6 |
| Number of blades | 3 |
| Blades torsion angle | 54.16$^o$ |
| Chord | 0.2 $m$ |
| Optimal tip speed ratio ($\lambda$) | 2.5 |
| Maximum power coefficient ($C_P$) | 0.41 |

the mathematical model on the H-type turbine have a greater discrepancy probably due to the lack of statistical model of turbulence. Although the results for the helical turbine are similar, it is necessary to increase the quality of the mesh, which would provide more realistic results and, quite possibly with lower power coefficient values. Table III summarizes the final parameters of the analyzed helical micro turbine.

## V. CONCLUSIONS

A double-multiple streamtube mathematical model developed in *Maltab®* code was tested on a micro vertical-axis wind turbine, helical-type, with acceptable results. The trend in power coefficient values is close to the trend values obtained in similar experimental result reported in literature.

The micro wind turbine was also analyzed by using CFD simulation with *Fluent ANSYS®*. Simulation results indicate that with a solidity of 0.6 and a chord of 0.2 m, the 3-blades turbine presents the best performance, reaching a power coefficient of 0.39, with $\lambda$ range values from 1 to 3.5. For the same conditions, the mathematical model yields a maximum power coefficient of 0.41, not including turbulence, considered as an acceptable result for modeling values.

The code algorithm allows a rapid estimation of turbine efficiency, which represents reduction of simulation time. However a turbulence modeling is needed to improve the *Maltab®* code.

## REFERENCES

[1] J. Reneses and E. Centeno, "Impact of the Kyoto Protocol on the Iberian Electricity 2 Market: A scenario analysis," *Energy Policy*, Vol. 36, pp. 2376-2384, 2008.

[2] S.N. Chandramowli and F.A. Felder, "Impact of climate change on electricity systems and markets - A review of models and forecasts," *Sustainable Energy Technologies and Assessments*, Vol. 5, pp. 62-74, 2014.

[3] World Wind Energy Association, "2014, Half-year Report", 2014.

[4] World Wind Energy Association, "2015 Small Wind World Report Summary", March, 2015.

[5] G.J.M. Darrieus, *Turbine having its rotating shaft traverse to the flow of the current*, US Patent No. 1,835,018; 1931.

[6] W. Tjiu, T. Marnoto, S. Mat, M. H. Ruslan, and K. Sopian, "Darrieus vertical axis wind turbine for power generation I: Assessment of Darrieus VAWT configurations," *Renewable Energy*, Vol. 75, pp. 50-67, 2015.

[7] F. Scheurich, T.M. Fletcher, and R. E. Brown, "The influence of blade curvature and helical blade twist on the performance of a vertical-axis wind turbine," *29th ASME Wind Energy Symposium*, Jan. 4-7, 2010, Orlando, Florida.

[8] A.M. Gorlov, *Unidirectional reaction turbine operable under reversible fluid from flow*, US Patent No. 5,451,138; 1995.

[9] A.M. Gorlov *Unidirectional helical reaction turbine operable under reversible fluid flow for power systems*, US Patent No. 5,451,137; 1995.

[10] M. Sathyajith, *Wind Energy: Fundamentals, Resource Analysis and Economics*, Springer, 2006.

[11] M.H. Mohamed, "Performance investigation of H-rotor Darrieus turbine with new airfoil shapes," *Energy*, Vol. 47, pp. 522-530, 2012.

[12] I. Paraschivoiu, *Double-multiple streamtube model for studying vertical-axis wind turbines*, Polytechnic International Press, Canada,1988.

[13] I. Paraschivoiu, *Wind Turbine Design: With Emphasis on Darrieus Concept*, Polytechnic International Press, Canada, 2002.

[14] M.B. Patel and V. Kevat, "Performance prediction of straight bladed Darrieus wind turbine by single streamtube model," *International Journal of Advanced Engineering Technology*, Vol. 14, p. 2, 2013.

[15] I. Paraschivoiu. "Double-multiple streamtube model for Darrieus wind turbines." *DOE/NASA Wind Turbine Dynamics Workshop 2nd Cleveland*, pp. 19-24. 1981.

[16] E.E. Lapin, "Theoretical performance of vertical axis wind turbines," *ASME paper, 75-WA/Ener-1, The winter annual meeting*, Houston, TX, USA, 1975.

[17] M. Islam, D.S.K. Ting, and A. Fartaj, "Aerodynamic models for Darrieus-type straight bladed vertical axis wind turbines," *Renewable and Sustainable Energy Reviews*, Vol. 12, pp. 1087-1109, 2008.

[18] M.H. Mohamed, "Performance investigation of H-rotor Darrieus turbine with new airfoil shapes," *Energy*, Vol. 47, pp. 522-530, 2012.

[19] J.M.F. Oro, *Técnicas numéricas en ingeniería de fluidos: Introducción a la dinámica de fluidos computacional (CFD) por el método de volúmenes finitos*, Editorial Reverté, S.A., Barcelona, 2012.

[20] M.R. Castelli, A. Englaro, and E. Benini, "The Darrieus windturbine: proposal for a new performance prediction model based on CFD," *Energy*, Vol. 36, pp. 4,919-4,934, 2011.